Desalination and Water Treatment
www.deswater.com

doi:10.5004/dwt.2018.22911

125 (2018) 93–101
September

Removal of toxic methyl green (MG) in aqueous solutions by apricot stone activated carbon – equilibrium and isotherms modeling

Moussa Abbas[a,*], Tounsia Aksil[a], Mohamed Trari[b]

[a]*Laboratory of Soft Technologies and Biodiversity, Faculty of Sciences, University M'hamed Bougara of Boumerdes, Boumerdes 35000, Algeria, Tel. +213 552408419, Fax +213 21 24 80 08, email: moussaiap@gmail.com (M. Abbas), tounsiaiap@gmail.com (T. Aksil)*
[b]*Laboratory of Storage and Valorization of Renewable Energies, Faculty of Chemistry (USTHB), BP 32-16111 El-Alia, Algeria, email: solarchemistry@gmail.com (M. Trari)*

Received 24 January 2018; Accepted 3 August 2018

ABSTRACT

Apricot stone activated carbon (ASAC), was powdered, activated and to be used as effective adsorbent to remove the dyes from aqueous solutions through batch experiments under operational factors namely, pH, contact time, adsorbent dose, initial dyes concentration and temperature. The physico-chemical, morphological and structural properties of the adsorbents were characterized by scanning electron microscope (SEM) and X-ray diffraction (XRD) instruments. Different kinetic models indicated that the adsorption is well described by the pseudo-second order model. The isotherms of methyl green (MG) adsorption on ASAC were obtained and correlated with various models. The smaller RMSE values for the Langmuir and Dubinin-Radushkevic models indicated the best fitting; the mono layer adsorption capacity of MG was found to be 148.478 mg g^{-1} at 21°C and 88.11 mg g^{-1} at 46°C at pH 10. The thermodynamic functions showed spontaneous and endothermic MG adsorption. In conclusion, the adsorbent prepared from apricot stone (ASAC) was found to very effective and suitable adsorbent for reactive dyes removal from aquatic environment, due to its simple and cheap preparation, easy availability and good adsorption capacity.

Keywords: Apricot stone; Methyl green; Isotherm; Adsorption; Equilibrium; Thermodynamic

1. Introduction

The dyes production plants are increasing by the day with the technological advancement. Colored waste waters are the result of extensive dyes production, they come from the textile industries and cause hazards to the aquatic environment due to presence of acids, bases, toxic organic, inorganic, dissolved solids and color. Indeed, the landfill of dyes is worrying for both toxicological and esthetic reasons which affect the quality of the receiving streams and toxic to food chain organisms. These colored compounds are not only aesthetically displeasing but also inhibit considerably the penetration of the solar light in water, thus reducing the photosynthetic process. Many organic dyes are harmful to human and the removal of color from waste effluents becomes environmentally important [1]. Many physical and chemical techniques were used for the removal of effluents from the textile, leather, food processing, dyeing, cosmetics, paper and dye industries which represent the main pollution sources**.** The dyes are not easily degradable and cannot be eliminated by the conventional techniques including the coagulation [2] ozonation [3]. In this respect, the adsorption remains popular owing of its low cost, easy design, facile operation and adsorbent recycling [4]. The dyes accumulation in the water medium gives rise to a chemical oxygen demand, biochemical oxygen demand and high-suspended solids. In addition, the adsorption is an attractive alternative, particularly if the adsorbent is low cost and locally available. Activated carbon is a versatile adsorbent but is relatively expensive. Most commercial systems use activated carbons as sorbents for the pollutants uptake in wastewater, which remains expensive. Therefore, the dyes adsorption on various materials have been extensively studied, and

*Corresponding author.

the activated carbons have proved is effectiveness because of its high specific surface area, large adsorption capacity and low selectivity for ionic and non ionic dyes [5]. Accordingly, many researchers have investigated the feasibility of abundantly available substances for the preparation of activated carbons. Accordingly, this has prompted a growing interest in the production of activated carbons from renewable and cheaper precursors which are either agricultural or industrial by-products. However, the available activated carbons are relatively expensive and the cost of their production and regeneration are limiting parameters**.** Hence, the environmental research was focused on new low-cost precursors especially those issued from agricultural wastes like rubber seed coat [6], olive stones [7], oil palm fiber [8] and apricot stone [9]. The great adsorption capacity of activated carbons is attributed to their developed porous structure, pore size distribution and surface functional groups. The adsorption yield strongly depends on the polarity, solubility, molecular size of adsorbate, pH and the presence of foreign ions in solution. However, the mechanism by which the adsorption of many compounds, particularly organic molecules, takes place on active carbons remains still unknown. Agricultural by-products exist in large quantities of apricot stones, produced annually in Algeria, and represent a solid pollutant for the environment during the last decades; these by-products were used as fuel in rural zones. Currently the preparation of activated carbon is greatly encouraged and apricot stone is a cheap precursor source for activated carbon and it was attractive to assess its capacity as adsorbent [10]. The advantage of abundant and available residual apricot stone, as raw material provides a further economic interest. The apricot stone used in this work was prepared by chemical and physical activations and this research was carried out in order to optimize the initial dye concentration, pH, grain size, contact time, adsorbent dose, agitation speed and temperature. In addition, the equilibrium adsorption data were fitted by various models to get constants related to the adsorption process. The equilibrium and kinetic analysis were undertaken to determine the factors controlling the biosorption rate, to optimize the physical parameters in the dye uptake and to find out the possibility of using this material as low-cost biosorbent for dye removal.

2. Experimental

2.1. Materials and methods

Analytical grade reagents were used in this research, the basic dye, MG (99%) was provided from Merck Company and its spectrum of MG at different pH is given in Fig. 1. Activated carbon was prepared by the carbonization and chemical activation with H_3PO_4 (85%) : Apricot stones obtained from Algiers region, were air-dried, crushed and screened to have two fractions with average sizes of 63 and 2.5 mm. 100 g of the selected fraction are impregnated with concentrated H_3PO_4 and dried in air. Then, the apricot stones were activated in a muffle furnace oven at 250°C (4 h). The carbonized material was thoroughly washed with distilled water to remove the acid until the pH reaches 6.8 and dried at 105°C. The clean biomass was mechanically ground and sifted to get powders of different grains sizes: 63 µm to 2 mm.

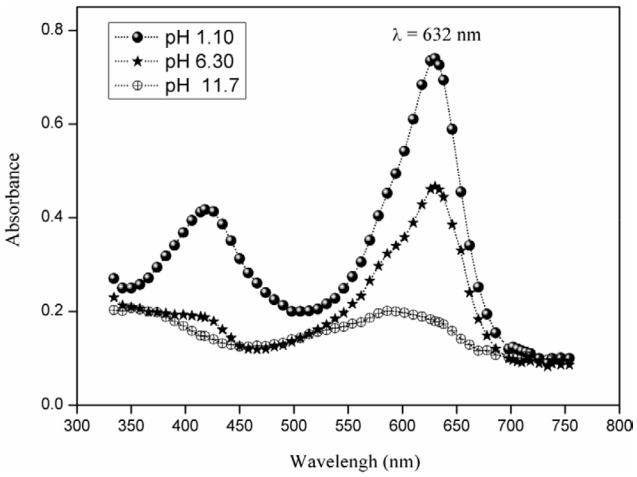

Fig. 1. Uv-visible spectrum of MG at different pH.

2.2. Activated carbon characterization

The synthesized activated carbon was characterized (bulk density and surface area), chemical and adsorption properties (point of zero charge: pH_{pzc}).

The analysis was determined with an elemental analyzer LECO-CHNS 932.

The specific surface area of the activated carbon was measured by the BET-technique, using N_2 at 77 K and a Pore Size Micrometric-9320.

The ash content (%) was determined by heating the activated carbon at 450°C for 3 h. The electrical conductivity was measured with a conductimeter type Erwika.

The point of zero charge pH_{pzc} of ASAC was determined by using 20 mL of KNO_3 solution (0.01 M), in closed conical flasks. The pH was adjusted between 2 and 14 by addition of HCl (0.1 M) or NaOH (0.1 M). Then, 0.1 g of ASAC was added and the final pH was taken after 24 h under agitation at ambient temperature. pH_{pzc} corresponds to the intersection of the curves of final pH and initial pH intersect.

The infrared data of ASAC were recorded with IR spectrometer FT Bomen-Michelson type; the spectra were obtained by grinding ASAC (2%) with KBr(spectroscopic quality). The mixture was pressed into pellets (Φ = 1 cm) under a uniaxial pressure of 2 tons cm^{-2}.

The X-ray diffraction (XRD) of the native apricot stone (NAS) and ASAC were recorded with a Philips X-ray diffractometer (PW 1890 model) using Cu Kα radiation (40 kV, 40 mA, λ = 1.5418 Å). The pattern were obtained with CONIT T-2T scan mode at 0.17 deg $step^{-1}$ of step width and 8° min^{-1}. The morphology of ASAC before and after biosorption MG molecules was visualized with a scanning electron microscopy with different resolutions using a JOEL-5910.

2.3. Batch mode adsorption studies

The effects of the initial MG concentration (C_o, 30–120 mg L^{-1}), pH (2–14), adsorbent dose (1–10 g L^{-1}),

agitation speed (100–1200 rpm) and temperature (298–338 K) on the MG adsorption were investigated in batch configuration for variable specific periods (0–60 min). The MG stock solution was made up by dissolving the accurate amount of MG (99%) in distilled water, the solutions down to 30 mg L^{-1} were prepared by dilution; pH was adjusted with HCl (0.1 mol L^{-1}) or NaOH (0.1 mol L^{-1}). For the kinetic studies, desired quantities of ASAC were contacted with 10 mL of MG solutions in Erlenmeyer flasks and placed on a rotary shaker at 300 rpm, the aliquots were withdrawn at regular times and subjected to a vigorous centrifugation at 3000 rpm (10 min). The remaining MG concentration was titrated with a Perkin Elmer UV-visible spectrophotometer model 550S at (λ_{max} = 632 nm). The amount of MG ions adsorbed q_t (mg·g^{-1}) by ASAC was calculated from the relation:

$$q_t = \frac{(C_o - C_e)V}{m} \quad (1)$$

C_o is the initial MG concentration and C_t the MG concentrations (mg L^{-1}) at time (t), V the volume of solution (L) and m the mass of ASAC (g). Because of the inherent bias resulting from linearization of isotherm models, the non-linear regression root mean square error (RMSE) equation [Eq. (2)], the sum of error squares (SSE) equation [Eq. (3)] and Chi-squares (X^2) equation [Eq. (4)] test were used as criteria for the fitting quality. The smaller RMSE value indicates the better curve fitting [7].

$$RMSE = \sqrt{\frac{1}{N-2}\sum_1^N (q_{e,\exp} - q_{e,cal})^2} \quad (2)$$

$$SSE = \frac{1}{N}\sum_{N=1}^{\infty}\left(q_{e,cal} - q_{e,\exp}\right)^2 \quad (3)$$

$$X^2 = \sum_1^N \frac{\left(q_{e,\exp} - q_{e,cal}\right)^2}{q_{e,cal}} \quad (4)$$

where $q_{e(ex)}$ (mg·g^{-1}) is the uptake experimental, $q_{e(cal)}$ the calculated value of uptake using a model (mg·g^{-1}) and N the number of observations in the experiment (the number of data points). The smaller RMSE value indicates the better curve fitting.

3. Results and discussion

3.1. Characterization of ASAC

- The physical and chemical properties of ASAC as well as the elementary analysis are gathered in Table 1. The spectra Fig. 2 show a number of absorption peaks (3436, 2929, 1732, 1599 and 1508 cm^{-1}) indicating that many functional groups are present on the surface adsorbent [10]. The band in the region (3122–3680 cm^{-1}) is assigned to hydroxyl (–OH) groups (libber and intermolecular hydrogen band) while the peak 1732 cm^{-1} is due to C=O bond in the carboxylic groups. These results indicate that the carboxylic and hydroxyl groups are responsible of the MG bio sorption.
- Both XRD patterns of NAS and prepared ASAC (Fig. 3) do not contain any definite peak, suggesting that ASAC exhibits mostly an amorphous nature with a large specific surface area.

Table 1
Physical and chemical properties of the apricot stones activated carbon (ASAC)

Elemental analysis of ASAC (%) C: 48.45 H: 6.03 N: 0.44 O: 45.08	
pH_{zpc}	7.05 ± 0.10
Surface area (m^2/g)	88.05 ± 1.03
Average pore diameter (Å)	176.32 ± 0.25
Average pore volume (mL/g)	0.2641± 0.003
Conductivity (µS/cm)	112.0 ± 2
Humidity (%)	1.48 ± 0.16
The rate of ash (%)	1.68 ± 0.02
The percentage of organic matter (%)	98.32 ± 0.11

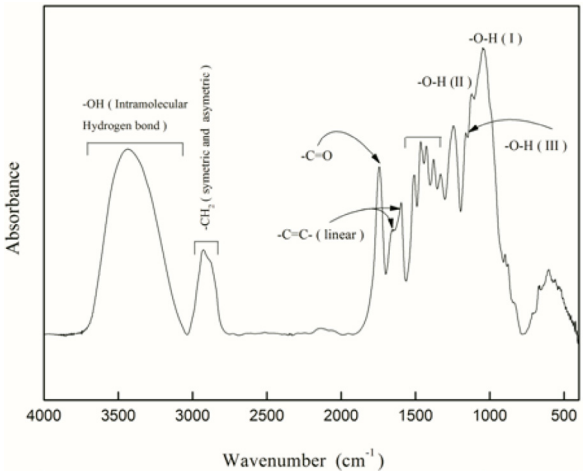

Fig. 2. Spectrum of FTIR analysis from ASAC.

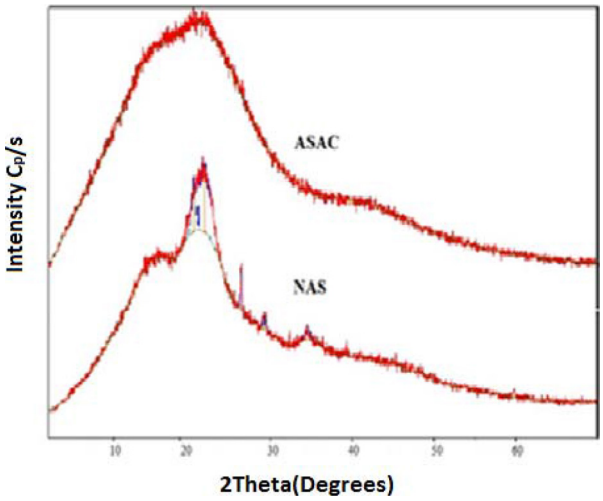

Fig. 3. X-ray paterns of the native apricot stone NAS and ASAC.

- SEM images of ASAC (Fig. 4) exhibits a micro porous nature with different pore diameters. Moreover, the ASAC surface is rough and presents many protrusions before adsorption. The morphology changed significantly after adsorption, and the surface became smoother with less visible pores, implying that the adsorption occurs on both the surface and inside the pores.

3.2. Effect of analytical parameters

3.2.1. Effect of ASAC size

In the first stage of batch adsorption tests on ASAC, the effect of grain sizes on the acid dye adsorption is studied. Significant changes in the uptake capacity and removal yields are observed for different grain sizes, indicating that the best adsorption occurs for lower sizes (315–800 µm). In general, smaller grains provide high specific surface areas, with a large dye uptakes and removal yields. The grain size range (315–800 µm) is subsequently used in the further adsorption experiments.

3.2.2. Effect of pH

The pH plays a key role in the MG adsorption by ASAC; the percentage of acid dye removal increases consistently with raising pH (Fig. 5). The influence of pH can be explained on the basis of pH_{zpc} = 7.05, for which the adsorbent surface is zero. The surface charge of the adsorbent is positive below pH_{zpc} and negative above pH_{zpc}. As the pH decreases, the number of positively charged sites increases and improves the MG adsorption by electrostatic attractions.

3.2.3. Effect of stirring speed

The maximum elimination was reached for an agitation speed of 300 rpm which gives a good homogeneity for the mixture suspension and prevents the Vortex phenomenon.

3.2.4. Effect of contact time and initial concentration

The MG adsorption capacity increases over time and reaches a maximum after 40 min, implying that no more MG ions are further adsorbed from the solution. The equilibrium time is found to be 40 min. The increase of the MG initial concentration (C_o) in the range 30–100 mg L^{-1} increases the adsorption from 10.08 to 34.51 mg g^{-1} (Fig. 6). This may be due to the increased driving force coming from the concentrations gradient with raising the concentration C_o to overcome the mass transfer resistance of MG ions at the interface solid/solution.

3.2.4. Effect of adsorbent dosage

For the first stage of batch adsorption tests on ASAC, the effect of adsorbent dose on the MG elimination is stud-

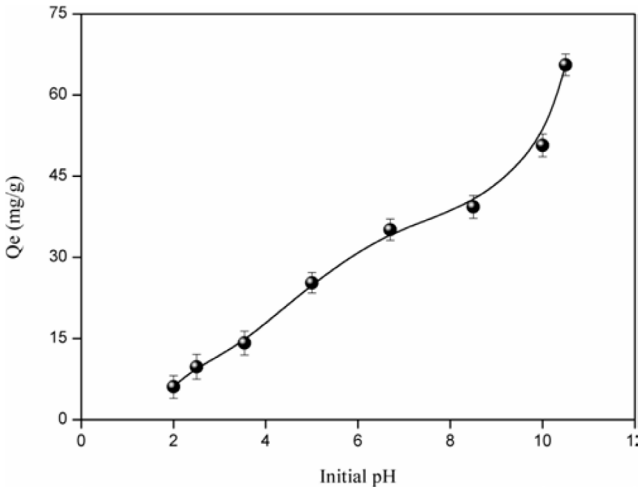

Fig. 5. Effect of pH on the MG adsorption efficiency (T: 21°C, C_0: 50 mg/L, contact time: 40 mn, stirring speed: 300 rpm and adsorbent dosage: 1 g/L and particle size: [315–800 µm]).

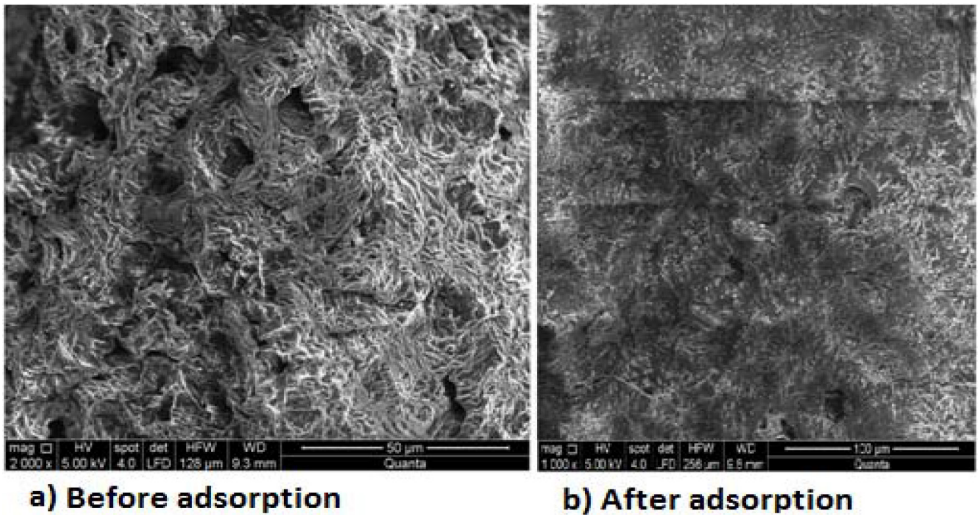

Fig. 4. Scanning electron micro graphs of ASAC after and before adsorption.

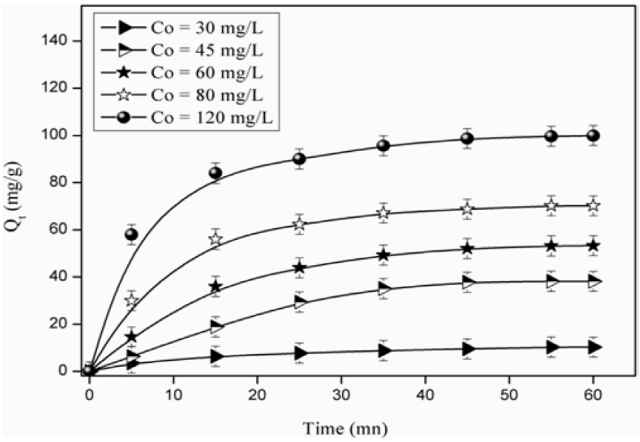

Fig. 6. Effect of the contact time on the adsorption of MG onto ASAC for different initial concentrations (T 21°C pH 10, contact time 40 mn, stirring speed 300 rpm, absorbent dosage 1g/L and particle size 315–800 µm).

ied. Significant changes in the removal capacity efficiency observed at different adsorbent doses (1–10 g L^{-1}) show that the best performance is observed for a dose of 1 g L^{-1}. Such result is expected because the removal yield is improved by the fact that higher the mass available, greater the contact surface offered to the adsorption. In addition, higher the dose of the adsorbent in solution, better the availability of exchangeable sites for ions, i.e. more active sites exist for binding of MG species. Our results agree with those obtained in the open literature and are consequently used in all isotherms adsorption experiments.

3.3. Adsorption isotherms

The shapes of the isotherms permit to diagnose the nature of adsorption phenomenon on the base of the classification of Giles et al.: L, S, H, and C [11]. The isotherms of ASAC at 21 and 46°C show L and S type (Figs. 7a and 7b). The initial part of the S curve shows a small interaction MG/carrier for low concentrations. However, as the concentration in the liquid phase increases, the adsorption occurs more readily. Such behaviour is attributed to a synergistic effect with the adsorbed dye, thus facilitating the adsorption of further molecules by attractive interaction; the equilibrium isotherm equations describe the experimental data. The parameters and the thermodynamic assumptions of these models provide insights into the adsorption, surface properties and adsorbent affinity. A better fitting of the isotherms is needed, because as further applications are developed, detailed isotherm descriptions are required for the adsorption designs.

The Langmuir model is extensively applied whose linearized form is given by [12]:

$$\frac{1}{q_e}=\frac{1}{q_{\max}}-\frac{1}{q_{\max}\cdot K_L\cdot C_e} \quad (5)$$

C_e is the equilibrium concentration (mg L^{-1}), q_{max} the monolayer adsorption capacity (mg/g) and K_L the Langmuir constant (L mg^{-1}) (Fig. 8). The applicability to

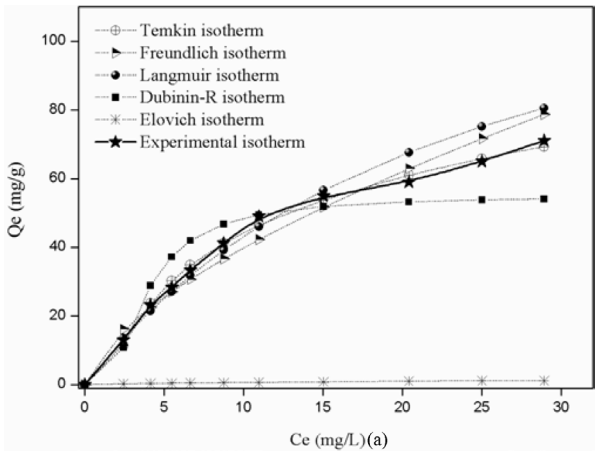

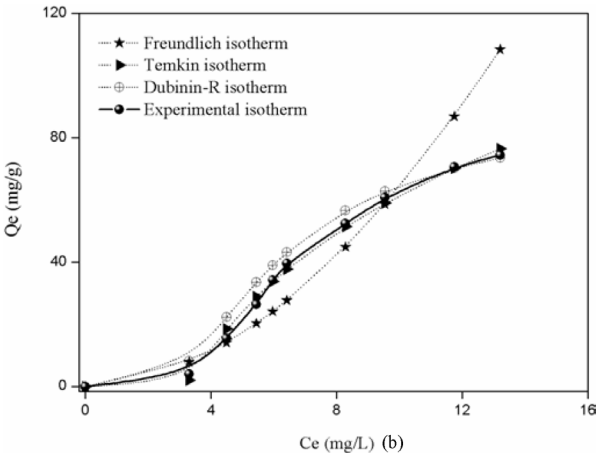

Fig. 7. (a) Adsorption isotherm of MG by ASAC at 21°C, (b) ASAC at 65°C.

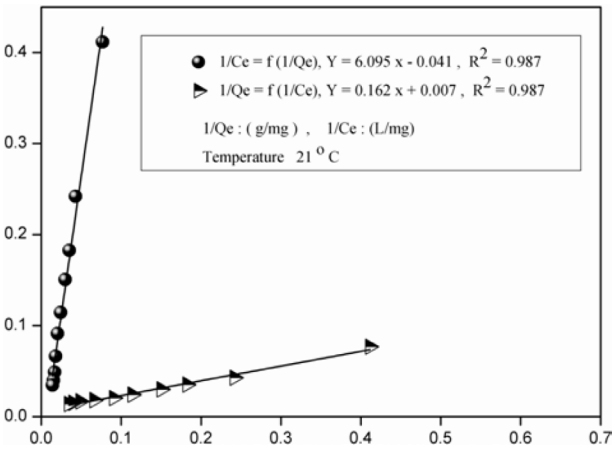

Fig. 8. The Langmuir isotherm for the adsorption of MG ions onto ASAC.

the adsorption is evaluated by evaluation of the statistic RMSE values. The smaller RMSE values obtained at 21°C for the models show a best fitting. The main feature of the model is the dimensionless constant (separation factor) [13]:

$$R_L = \frac{1}{1 + K_L \cdot C_o} \quad (6)$$

where C_o is the initial concentration of the adsorbate. R_L indicates the isotherm type: irreversible ($R_L = 0$), favourable ($0 < R_L < 1$), linear ($R_L = 1$) or inappropriate ($R_L > 1$). In our case, R_L is smaller than unity, confirming the favourable adsorption in both cases as well as the applicability of isotherm.

The Freundlich model is valid for non ideal adsorption on heterogeneous surfaces as well as multilayer adsorption is given by [12]:

$$Lnq_e = LnK_F + \frac{1}{n} \cdot LnC_e \quad (7)$$

The constant K_F indicates the adsorption capacity of the adsorbent (L g^{-1}) and n an empirical constant related to the adsorption driving force. The plot $Ln\ q_e$ vs. $Ln\ C_e$ permits the calculation of both the constant K_F and exponent n.

The Temkin model describes the adsorption on heterogeneous surfaces, applied in the following form [14]:

$$Q_e = \frac{RT}{b} LnA + \frac{RT}{b} LnC_e = BlnA + BlnC_e \quad (8)$$

The adsorption data are analyzed on the base of equation [Eq. (8)]. Therefore, the plot of q_e vs. $Ln\ C_e$ gives the constants A and B.

The Dubinin-Radushkevich (D-R) model is used to describe adsorption on both homogenous and heterogeneous surfaces; the linear form is expressed as follows [15]:

$$Lnq_e = Lnq_m - \beta \cdot \varepsilon^2 \quad (9)$$

q_m is the D-R monolayer capacity (mg g^{-1}), β a constant related to the adsorption energy, while the Polanyi potential ε is related to the equilibrium concentration:

$$\varepsilon = RTLn\left(1 + \frac{1}{C_e}\right) \quad (10)$$

β gives the average free energy (E) of adsorption per molecule when it is transferred to the surface of the solid from infinity in solution [16].

$$E = \frac{1}{\sqrt{2\beta}} \quad (11)$$

The magnitude of E is useful for evaluating the adsorption mechanism. $E < 8$ kJ·mol^{-1}, the physical forces affect the adsorption. Conversely, if E is in the range (of 8–16 kJ mol^{-1}), the adsorption is mainly governed by ion exchange mechanism [17].

The Elovich model assumes that the number of adsorption sites increases exponentially with the adsorption, implying a multilayer adsorption [17]:

$$In\frac{q_e}{C_e} = In\left(q_m \cdot K_E\right) - \frac{q_e}{q_m} \quad (12)$$

where K_E (L mg^{-1}) is the Elovich constant at equilibrium, q_m (mg g^{-1}) the maximum adsorption capacity, q_e (mg g^{-1}) the adsorption capacity at equilibrium and C_e (g L^{-1}) the adsorbate concentration at equilibrium.

If the adsorption is described by Eq. (12), K_E and q_m are determined from the curve $Ln\ (q_e/C_e)$ *vs.* q_e.

The theoretical parameters of adsorption isotherms with the coefficients, RMSE, SSE and X^2 are gathered in Table 2. The Langmuir isotherm shows higher values of RMSE, X^2 and SSE.

3.4. Adsorption kinetics

The adsorption kinetic describes the uptake rate of adsorbate and controls the time of the whole adsorption process. The pseudo first order and pseudo second-order are chosen for the adsorption description.

Table 2
Sorption isotherms coefficients of different models

Model	Langmuir	Freundlich	Temkin	Dubinin-R	Elovich
Type (V)	K_L: 0.0432 L/mg	K_F: 9.157 mg/g	B_T: 23.411	Q_M: 54.91 mg/g	Q_m: 65.274 mg/g
	Q_m: 148.478 mg/g	1/n: 0.6394	K_T: 0.668 L/mg	K: 13.66 mol^2 K/j	K_E: 0.121 L/mg
21°C	K_L: 0.04105 L/mg		ΔQ: 15.503 kJ/mol	E: 661.351 J/mol	
Type (I)	Q_m: 142.65 mg/g				
R^2	0.98656	0.94704	0.99152	0.8471	0.84591
RMSE	41.144	20.484	2.002	87.562	1658.00
SSE	1692.79	419.594	4.008	7667.104	2748964
X^2	0.544	0.340	0.077	1.597	1163.788
46°C		K_F: 0.833 mg/g	B_T: 53.647	Q_m: 88.111 mg/g	
		1/n: 1.887	K_T: 0.315 L/mg	K: 33.912 mol^2 K/J	
			ΔQ: 4.355 kJ/mol	E: 455.43 J/mol	
R^2		0.83692	0.99946	0.99826	
RMSE		352.927	3.051	18.462	
SSE		124552.5	9.3087	340.845	
X^2		3.289	0.586	0.8756	

The pseudo first order equation [18]:

$$\log\left(q_e - q_t\right) = \log q_e - \frac{K1}{2.303}\cdot t \tag{13}$$

The pseudo second order model [19,20]:

$$\frac{t}{q_t} = \frac{1}{K_2 \cdot q_e^2} + \frac{1}{q_e}\cdot t \tag{14}$$

q_t (mg g^{-1}) is the adsorbed at time t (min), K_1 and K_2 the rate constants of the pseudo-first (min^{-1}) pseudo-second order kinetics (g mg^{-1} min^{-1}) respectively. The experimental data deviate greatly from the linearity for the pseudo-first order kinetic as evidenced by the low q_e values, indicating the inapplicability of the model. By contrast, the $q_{e'cal}$ value of the pseudo-second order kinetic model agrees with the experimental results (Table 3).

3.5. Intra particle diffusion study

The functional relationship common to most adsorption processes varies almost proportionally with $t^{1/2}$, the Weber-Morris plot (q_t versus $t^{1/2}$) (Fig. 9) rather than with the constant time t [21].

$$q_t = K_{\text{in}}\, t^{1/2} + C \tag{15}$$

K_{in} is the intra particle diffusion rate constant. The intercept C gives an idea about the thickness of the boundary layer [22]. This is due to the instantaneous utilization of the readily available adsorption sites on the surface. K_{in} and C are deduced from the slope and intercept of linear plots, the constant of the modified Freundlich and Elovich models are gathered in Table 3.

3.5.1. Adsorption mechanism

The mechanisms and kinetics of the adsorption are described by various models, which predict the breakthrough curves at different times and accuracies. Nevertheless, there are not clear criteria to decide which model is convenient for a given case:

- The involved mass transfer resistances
- Relation type between the adsorbed amount and the diffusion coefficients
- Definitive equilibrium equation
- Description level and mathematical complexity of the model

It is well known that a performed batch experiment gives valuable data to evaluate the diffusion coefficients. Under real conditions, the mass transport resistance in the solid is larger than the external fluid film on the solid particles.

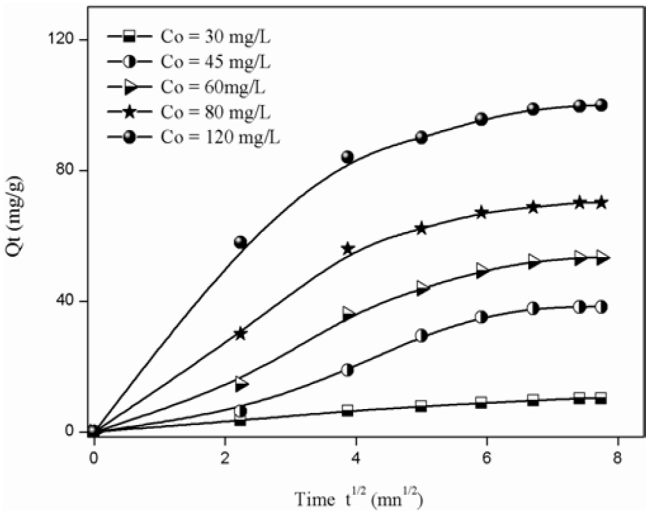

Fig. 9. Intraparticle diffusion effect on the adsorption of MG ion on ASAC (C_o: 50 to 100 mg/L, pH : 10, adsorbent dosage 1 g/L, particle size: [315–800] µm temperature: 21°C, stirring speed: 300 rpm and contact time: 40 mn).

Table 3
Kinetic parameters for adsorption of MG ions onto ASAC

		Pseudo-first order kinetic				Pseudo-second order kinetic			
C_o (mg/L)	Q_{exp} (mg/g)	K_1 (mn^{-1})	R^2	Q_{cal} (mg/g)	$\Delta Q/Q$ (%)	K_2 (g/mg·mn)	R^2	Q_{cal} (mg/g)	$\Delta Q/Q$ (%)
30	10.25	0.054	0.993	9.0780	11.43	0.00704	0.997	11.11	7.74
60	53.20	0.088	0.967	67.608	21.30	0.00133	0.989	55.56	4.24
80	70.17	0.082	0.998	54.954	27.68	0.00231	0.998	71.42	1.75
120	99.93	0.096	0.992	81.940	21.95	0.00215	0.999	107.18	6.76

		Intra particle diffusion			Modified Freundlich			Elovich model		
C_o (mg/L)	R^2	C (mg/g)	K_{in} (mg/g mn$^{1/2}$)	Diffusion D (cm^2. s^{-1})	K_F (mn·L/mg)	1/m	R^2	1/β (mg/g mn)	α (g/mg)	R^2
30	0.997	0.0279	1.575	5.18 10^{-6}	0.061	0.432	0.982	2.7790	0.123	0.998
45	0.957	–1.427	5.721		0.015	0.726	0.934	13.736	8.10 E-9	0.975
60	0.977	0.159	8.931		0.126	0.508	0.906	15.793	1.07 E-5	0.976
80	0.977	1.066	12.97		0.246	0.329	0.882	15.954	231.46	0.939
120	0.922	6.870	18.42		0.362	0.214	0.926	16.744	5.15 E13	0.958

When the intra particules diffusion does not predominate the adsorption mechanism, a competition between the different processes is envisaged among which we can mention:

- Ion exchange adsorption.
- Adsorption by electrostatic forces.
- Adsorption by pooling a pair of electrons.
- Adsorption by hydrogen bonds.

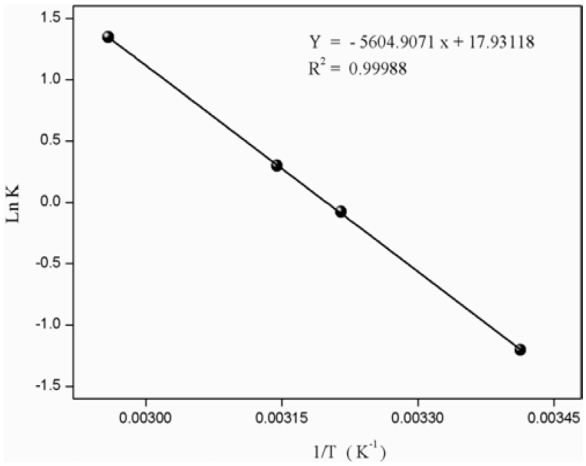

Fig. 10. Thermodynamic parameters, enthalpy and entropy for the adsorption of MG ions onto ASAC.

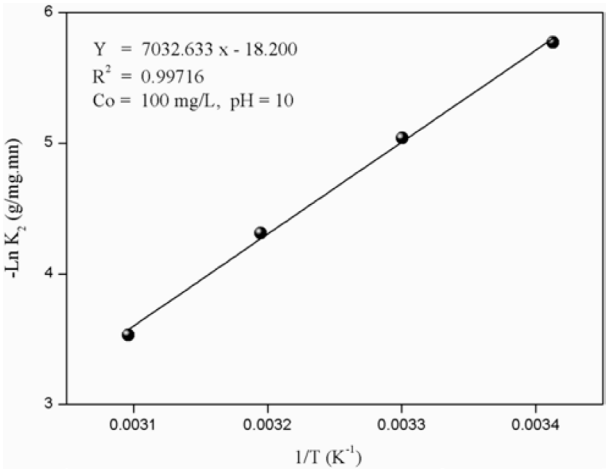

Fig. 11. Determination of activated energy.

3.6. Effect of temperature

The uptake capacity of ASAC decreases from 21.64 to 7.33 mg g^{-1} in the range 295–323 K, indicating that the adsorption is less favorable at high temperature. The thermodynamic functions i.e. the free energy (ΔG°), enthalpy (ΔH°) and entropy (ΔS°) are obtained from the following equations [23,24]:

$$\Delta G° = -RTLnK \quad (16)$$

$$\Delta G° = \Delta H° - T\Delta S° \quad (17)$$

The equilibrium constant (K) for the sorption is determined from the extrapolation to zero q_e of the plot

ln q_e/C_e versus q_e while ΔH°, ΔS° and activated energy E_a are deduced from the slope and intercept of the plots of Ln K versus 1/T (Fig. 10) and Ln K_2 = f (1/T) (Fig. 11) respectively**.** While the ΔG° ΔH°, ΔS° and Ea values at different temperatures are given in Tables 4 and 5.

3.7. Performance of the prepared ASAC

The adsorption capacity (q_{max}) is a comparative parameter and its value agrees with that reported in most previous works, indicating the easy adsorption onto our ASAC. This clearly shows that the apricot stone, very abundant in Algeria, is a free and effective adsorbent for MG. ASAC could be an attractive adsorbent for heavy metals and basic dyes owing to the isoelectric point (pH_{pzc}) and one of the perspectives is to achieve the adsorption experiments in column mode with industrial effluents. Preliminary tests are satisfactory; the experiments are currently under way and will be reported very soon in a next paper.

4. Conclusions

This study was devoted to the activated carbon prepared from apricot stone, employed as effective adsorbent for the removal of Methyl Green in aqueous medium.

The Dubinin-R and Langmuir models gave a better fit of the equilibrium adsorption data. They provided a maximum adsorption capacity of 148.47 mg g^{-1} at 21°C and decreased down to 88.11 mg g^{-1} at 65°C at pH ~10. The pseudo-second order model showed the best description of the kinetic data.

The negative free energy ΔG° and positive enthalpy ΔH° indicate that the MG adsorption on ASAC is spontaneous and endothermic over the investigated temperature range.

Table 4
Effect of temperature for the MG adsorption on ASAC

T (K)	Q_e (mg/g)	1/T (K^{-1})	K_2 (L/mg.mn)	R^2	–Ln K_2	Activation energy (kJ/mol)
293	45.25	$3.41296\ 10^{-3}$	$3.10\ 10^{-3}$	0.98739	5.7700	
304	66.22	$3.30033\ 10^{-3}$	$6.48\ 10^{-3}$	0.99966	5.0380	
313	85.65	$3.19488\ 10^{-3}$	$13.35\ 10^{-3}$	0.99967	4.3155	58.52
323	92.17	$3.09597\ 10^{-3}$	$29.14\ 10^{-3}$	0.99989	3.5330	

Table 5
Thermodynamic parameters for the MG adsorption on ASAC

T (K)	K	R^2	$1/T$ (K^{-1})	Ln K	ΔG (KJ/mol)	ΔH (KJ/mol)	ΔS (J/K mol)
293	0.30014	0.9994	$3.41\ 10^{-3}$	–1.2035	2.922		
311	0.92590	0.9999	$3.22\ 10^{-3}$	–0.0769	0.238		
318	1.34890	0.9999	$3.14\ 10^{-3}$	0.2993	–0.805	46.599	149.079
338	3.84316	0.9999	$2.96\ 10^{-3}$	1.3400	–3.786		

The positive entropy ΔS° showed that the randomness increases at the solid-solution interface during the MG adsorption, suggesting that some structural exchange occurred among active sites of adsorbent/MG ions.

The MG adsorption obeys to a pseudo-second order kinetic, and the chemisorption is the rate-limiting step. The MG ions are linked to the adsorbent surface by chemical bonds and tend to find sites that optimize their coordination number on the surface. The kinetic and thermodynamic data can be exploited for the design of adsorbent for the treatment of real effluents.

This work in tiny batch gave rise to satisfactory results, and our perspective will concentrate on the adsorption tests in column mode using industrial effluents treatment and the present contribution showed that ASAC is potentially a useful adsorbent for the heavy metals, acid and basic dyes.

References

[1] A.B. Karim, B. Mounir, M. Hachkar, M. Bakasse, A. Yaacoubi, Adsorption of malachite green dye onto raw Moroccan clay in batch and dynamic system, Canad. J. Environ. Constr. Civil Eng., V2, N2 (2011) 1–5.

[2] O. Tunay, Color removal from textile waste waters, Water Sci. Technol., 34(11) (1996) 9–16.

[3] P.L. Alioui Guillaume, A.-M. Chelaru, M. Visa, O. Lassiné, Titanium oxid-clay as adsorbent and photocatalysts for wastewater treatment, J. Membr. Sci. Technol., 8(1) (2018) 1–11.

[4] M.A. Malan, S. Ijaz, M.N. Ashiq, Removal of various dyes from aqueous media onto polymeric gels by adsorption process: their kinetics and thermodynamics, Desalination, 263 (2010) 249–257.

[5] S. Őzcan, B. Erdem, A. Özcan, Adsorption of acid Blue 193 from aqueous solutions onto Nabentonite and DTMA- bentonite, J. Colloid Interf. Sci., 280 (2004) 44–54.

[6] S. Rengaraj, S.H. Moona, R. Sivabalan, B. Arabindoo, V. Murugesan, Removal of phenol from aqueous solution and resin manufacturing industry wastewater using an agricultural waste: rubber seed coat, J. Hazard. Mater., B89 (2002) 185–196.

[7] A. Moussa, C. Abdelhamid, K. Samia, A. Tounsia, T. Mohamed, Kinetic and equilibrium studies of Coomassie Blue G-250 adsorption on apricot stone activated carbon, J. Environ. Anal. Toxicol., 5 (2015) 264.

[8] I.A.W. Tan, B.H. Hameed, A.L. Ahmad, Equilibrium and kinetic studies on basic dye adsorption by oil palm fibre activated carbon, Chem. Eng. J., 127 (2007) 111–119.

[9] M. Abbas, M. Trari, Kinetic, equilibrium and thermodynamic study on the removal of Congo Red from aqueous solutions by adsorption onto apricot stone, Process Safe. Environ. Protect., 98 (2015) 436–446.

[10] M. Abbas, S. Kaddour, M. Trari, Kinetic and equilibrium studies of cobalt adsorption on apricot stone activated carbon, J. Ind. Eng. Chem., 20 (2014) 745–751.

[11] C.H. Giles, T.H. Mac Ewan, S.N. Nakhwa, D. Smith, Studies in adsorption. Part XI. A system of classification of solution adsorption isotherms, and its use in diagnosis of adsorption mechanisms and in measurement of specific surface areas of solids, J. Chem. Soc., 10 (1960) 3973–3993.

[12] C. Gerent, V.K.C. Lee, P. Le clorrek, G. McKay, Application of chitosan for the removal of metals from waste waters by adsorption - Mechanisms and models review, Crit. Rev. Environ. Sci. Technol., 37 (2007) 41–121.

[13] F. Ogata, N. Nagai, N. Kawasaki, Adsorption capability of cationic dyes methylene Blue and crystal violet onto poly-y- glutamic acid, Chem. Pharm. Bull., 65(3) (2017) 268–275.

[14] S.J. Allen, G. McKay, J.F. Porter, Adsorption isotherm models for basic dye adsorption by peat in single and binary component systems, J. Colloid Interf. Sci., 80 (2004) 222–233.

[15] T. Shahwan, H.N. Erten, J. Radioanal, Temperature effects in barium sorption on natural kaolinite and chlorite-illite clays, Nucl. Chem., 260 (2004) 43–48.

[16] S.-H. Lin, R.-S. Juang, Heavy metal removal from water by sorption using surfactant-modified montmorillonite, J. Hazard. Mater., 92 (2002) 315–326.

[17] M. El Alouani, S. Alehyen, M. EL Achouri, M. Taibi, Removal of cationic dye – Methylene Blue- from aqueous solution by adsorption on fly ash-based geopolymer, J. Mater. Environ. Sci., 9 (2018) 32-46-97.

[18] S. Lagergren, About the theory of so-called adsorption of soluble substances, K. Sven. Ventensskapsakad. Handlingar Band, V., 24 (1998) 1–39.

[19] Y.S. Ho, G. Mc Kay, The kinetics of sorption of divalent metal ions onto sphagnum moss peat, Water Res., 34(3) (2000) 735–742.

[20] Y.S. Ho, G. McKay, Pseudo-second order model for sorption processes, Press Biochem., 34(5) (1999) 451–465.

[21] M.J. Weber, J. Morris, Kinetic of adsorption on carbon from solution ASCE, J. Sanit. Eng. Div., 89 (1963) 31–51.

[22] N. Kannam, M.M. Sundaram, Kinetics and mechanism of removal of Methylene Blue by adsorption on various carbon-a comparative study, Dyes Pigm., 51(1) (2001) 25–40.

[23] A. Demirbas, A. Sari, O. Isildak, Adsorption thermodynamic of steric acid onto bentonite, J. Hazard. Mater., B, 135 (2006) 226–231.

[24] M. Abbas, T. Aksil, M. Trari, M.R. Belmecheri, Equilibrium and isotherm modeling of toxic dye adsorption onto modified apricot stone, Adv. Environ. Waste Manage., 1(1) (2018) 1–6.